A General Theory for Equivalent Barotropic Thin Jets*

BENOIT CUSHMAN-ROISIN

Thayer School of Engineering, Dartmouth College

LARRY PRATT AND ELISE RALPH

Woods Hole Oceanographic Institution, Woods Hole, Massachusetts

(Manuscript received 30 October 1991, in final form 20 March 1992)

ABSTRACT

The so-called thin-jet approximation, in which variations along the jet axis are assumed gradual in comparison with variations normal to the axis, allows the calculations of along- and cross-axis structures to be decoupled. The result is a nonlinear equation, with one lesser spatial dimension, governing the meandering of the jet. Here a new such "path equation" is constructed in the context of a one-layer, reduced-gravity model. The formalism retains two distinct physical processes: a vortex-induction mechanism, originating from the jet curvature, that causes meanders to travel downstream (i.e., usually eastward), and the planetary (beta) effect, induced by meridional displacements, that gives the meanders the allure of Rossby waves and generates a westward (i.e., usually upstream) propagation.

After a brief comparison with previous path equations, analytical solutions of the new equation are explored, including solitons and other exact nonlinear wave forms. The presentation concludes with numerical experiments and a brief application to the Gulf Stream.

1. Introduction

Thin-jet models have been employed by a number of investigators in the study of meandering and eddy detachment processes (e.g., Warren 1963; Robinson and Niiler 1967; Robinson et al. 1975; Flierl and Robinson 1984; Pratt 1988). The thin-jet approximation, in which variations along the jet axis are assumed gradual in comparison with variations normal to the axis, allows the calculations of along- and cross-axis structures to be decoupled. The consequent mathematical simplifications often allow a semianalytic description of nonlinear meandering in which the motion of the axis is governed by a "path equation." Applications include eddy detachment in currents such as the Gulf Stream, where the ring-forming meanders often have wavelengths much larger than the stream width.

The most recent advancements in thin-jet theory have occurred along two lines of investigation. The first, more traditional, approach involves manipulations of the equations of motion in a natural coordinate system. The path equation is obtained by formulating a vorticity equation and integrating it over a section normal to the jet axis. The most comprehensive treatment, that of Flierl and Robinson (1984, hereafter FR), describes a Boussinesq, β-plane jet flowing over a horizontal bottom.

The second approach is based on the formulation of equations describing potential vorticity fronts in quasigeostrophic flows. Pratt and Stern (1986, hereafter PS) consider a single front separating two semi-infinite regions of uniform potential vorticity in an equivalent barotropic (1 1/2-layer) system. When the typical radius of curvature of the front is large compared to the Rossby radius of deformation, the integro–differential equation describing the motion of the front can be reduced to a relatively simple (looking) differential equation. In this limit the horizontal velocity field takes the form of a thin jet whose axis is the potential vorticity front. Pratt (1988) has shown that an equation of the same form will govern the long-wave behavior of any front whose motion is invariant to rotation or translation and whose position is independent of z.

A further advance in the long-wave theory of potential vorticity fronts has recently been made by Pedlosky (1990). Using 1 1/2-layer stratification and semigeostrophic β-plane dynamics, he analyzes a front with initial north–south alignment. A fundamental difference between this and other calculations, including the present, is that velocity discontinuities (equivalent to delta function in the potential vorticity field) are allowed in the former. A new time scale, inversely proportional to the velocity jump, is introduced, and the

* Woods Hole Oceanographic Institution Contribution No. 8021.

Corresponding author address: Dr. Larry Pratt, Woods Hole Oceanographic Institution, Clark-3, Woods Hole, MA 02543.

system is governed by a first-order hyperbolic equation that admits classical wave steepening. In the present calculation, where velocity continuity is assumed, the time scale is proportional to the cube of the characteristic meander wavelength. Associated with this longer scale is a more delicate dynamical balance governed by a higher-order equation.

It is natural to ask whether the equation obtained by Pratt (1988) is a special case of the (apparently) more general result of FR. Mysteriously, the former contains a term not present in the final equation of FR, and it is apparently not possible to perform the reduction. Since the derivations of the two results are so dissimilar, the basis for this disparity has not been obvious. Here we present several new results that generalize the theory of Pratt (1988), clarify the connection with FR, and suggest a concrete procedure for obtaining analytical solutions for a large class of initial conditions. Specifically, we extend the equivalent barotropic calculation of Pratt (1988) to β-plane and nonquasigeostrophic dynamics, including outcropping of the density interface. The results, presented in section 2, show that the equation of PS is obtained with the addition of a Doppler-shift term due to the β effect. Furthermore, the new result can be transformed into the modified KdV (Korteweg–deVries) equation, with path curvature the dependent variable and time and arc length the independent variables. When transformed back to Cartesian coordinates, the soliton solutions to this equation may contain "loops" associated with self-intersections of the path. Since the number and size of solitons arising from isolated initial disturbances can be predicted using an inverse scattering transformation, a method for predicting eddy detachment can be devised (section 5). Finally, we show that the present 1 1/2-layer model contains a vortex-stretching effect that is absent in FR and that accounts for the novel term in our path equation. The details of this dichotomy and the implied physics are described in section 3.

2. A semigeostrophic model

As a model of the upper ocean away from lateral boundaries and without bottom influence, consider a reduced-gravity system on the beta plane. With a reference depth H, such as the depth of the interface in a quiescent region, the reduced-gravity constant g' and the reference Coriolis parameter f_0 combine to provide the horizontal length $R_d = (g'H)^{1/2}/f_0$ (none other than the deformation radius) and the velocity $c = (g'H)^{1/2}$ (the gravity-wave speed). Using these quantities as scales, the primitive equations can be expressed in dimensionless form as follows:

$$u_t + uu_x + vu_y - (1 + \beta y)v = -h_x \quad (2.1)$$

$$v_t + uv_x + vv_y + (1 + \beta y)u = -h_y \quad (2.2)$$

$$h_t + uh_x + vh_y + h(u_x + v_y) = 0. \quad (2.3)$$

In these equations u and v are the velocity components in the x (eastward) and y (northward) directions, h is the interfacial depth, subscripts denote derivatives, and the coefficient β, defined by

$$\beta = \frac{R_d}{f_0}\frac{df}{dy} \quad (2.4)$$

and taken as a constant, measures the relative importance of the planetary (beta) effect. To validate the use of Cartesian coordinates, and because our interest lies in scales much less than the size of the earth, we shall take

$$\beta \ll 1. \quad (2.5)$$

In such a model, a jet is represented by a flow field in geostrophic balance with a pressure gradient; the latter being maintained by an interfacial slope connecting two reservoirs of uniform but different depths. If the distance over which the layer thickness varies from one value to the other (typically on the order of the deformation radius) is relatively short compared to the length over which meanders occur, the jet can be said to be narrow.

To take full advantage of the disparity of scales in the directions across and along the jet, a change of variables is in order. In the spirit of Flierl and Robinson (1984) and predecessors, but with slight modification, we define a time-dependent, curvilinear system of coordinates tied to the meandering jet (Fig. 1). A midjet curve, to be defined precisely later, is introduced, along which distance is measured by the variable s; at each point along the curve, a local normal is constructed, defining the variable n. For convenience, we take s increasing downstream and n increasing to the left facing downstream. Any point of coordinates (x, y) in the two-dimensional framework of reference can be

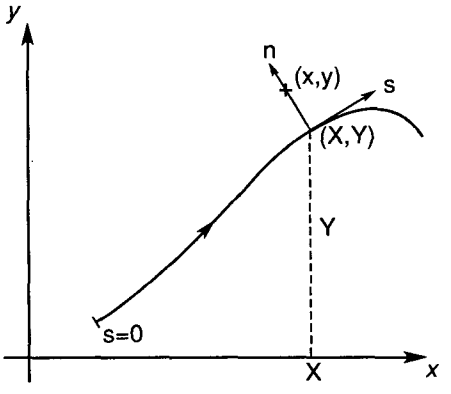

FIG. 1. Definition of the natural coordinates: s measures the distance along the midjet line from some origin, while n measures the distance from that curve, positively to the left, to any point (x, y) in the plane. The point (X, Y) is the point on the midjet line that is closest to the arbitrary point (x, y).

attributed the coordinates (s, n), where n is the distance from the point to the nearest point (X, Y) on the jet and s is the distance along the jet axis from an origin to that point (X, Y) (Fig. 1). The relations are

$$x = X - n\frac{\partial Y}{\partial s} \tag{2.6}$$

$$y = Y + n\frac{\partial X}{\partial s}, \tag{2.7}$$

where $X(s, t)$ and $Y(s, t)$ are thus the coordinates of the point on the midjet curve that is closest to the arbitrary point (x, y). The spatiotemporal functions $X(s, t)$ and $Y(s, t)$ describe the evolution of the midjet line, and the formulation of their evolution equations is the object of the model. Because s is the distance along the curve $(dX^2 + dY^2 = ds^2)$, the following geometric relation,

$$\left(\frac{\partial X}{\partial s}\right)^2 + \left(\frac{\partial Y}{\partial s}\right)^2 = 1, \tag{2.8}$$

must hold everywhere and at all times. This statement can be interpreted as a choice of normalization of the variables s.

There are other noteworthy properties: (X_s, Y_s) is the unit vector tangential to the midjet curve, pointing in the positive s direction; $(-Y_s, X_s)$ is the unit normal vector pointing in the positive n direction; and the curvature is

$$K = \frac{\partial X}{\partial s}\frac{\partial^2 Y}{\partial s^2} - \frac{\partial^2 X}{\partial s^2}\frac{\partial Y}{\partial s}, \tag{2.9}$$

which takes on positive (negative) values if the jet curves to the left (right). It is straightforward to show that the second derivatives of the jet coordinates (X, Y) are related to their first derivatives via the curvature by

$$\frac{\partial^2 X}{\partial s^2} = -K\frac{\partial Y}{\partial s}, \quad \frac{\partial^2 Y}{\partial s^2} = K\frac{\partial X}{\partial s}. \tag{2.10}$$

Before proceeding with the change of variables, it is also convenient to define the local alongjet and crossjet velocity components, U and V, respectively:

$$u = U\frac{\partial X}{\partial s} - V\frac{\partial Y}{\partial s} \tag{2.11a}$$

$$v = U\frac{\partial Y}{\partial s} + V\frac{\partial X}{\partial s}. \tag{2.11b}$$

The change of variables consists in the systematic replacement of the coordinates (x, y) by (s, n) and of the velocity components (u, v) by (U, V). The governing equations (2.1)–(2.3) are then transformed into the equivalent set:

$$\frac{\partial U}{\partial t} + \left(JU - A + nJ\frac{\partial C}{\partial s}\right)\frac{\partial U}{\partial s} + (V - C)\frac{\partial U}{\partial n} - \left[1 + J\frac{\partial C}{\partial s} + \beta\left(Y + n\frac{\partial X}{\partial s}\right) + JKU\right]V = -J\frac{\partial h}{\partial s} \tag{2.12}$$

$$\frac{\partial V}{\partial t} + \left(JU - A + nJ\frac{\partial C}{\partial s}\right)\frac{\partial V}{\partial s} + (V - C)\frac{\partial V}{\partial n} + \left[1 + J\frac{\partial C}{\partial s} + \beta\left(Y + n\frac{\partial X}{\partial s}\right) + JKU\right]U = -\frac{\partial h}{\partial n} \tag{2.13}$$

$$\frac{\partial h}{\partial t} + \left(JU - A + nJ\frac{\partial C}{\partial s}\right)\frac{\partial h}{\partial s} + (V - C)\frac{\partial h}{\partial n} + \left(J\frac{\partial U}{\partial s} + \frac{\partial V}{\partial n} - JKV\right)h = 0, \tag{2.14}$$

where the ancillary quantities $A(s, t)$, $C(s, t)$, and $J(s, n, t)$ are defined by

$$A = \frac{\partial X}{\partial t}\frac{\partial X}{\partial s} + \frac{\partial Y}{\partial t}\frac{\partial Y}{\partial s} \tag{2.15}$$

$$C = \frac{\partial X}{\partial s}\frac{\partial Y}{\partial t} - \frac{\partial X}{\partial t}\frac{\partial Y}{\partial s} \tag{2.16}$$

$$J = \frac{1}{1 - nK}. \tag{2.17}$$

Geometrically, A and C are the velocity components of the point (X, Y) in the tangential and normal directions, respectively (i.e., A is the sliding velocity and C is the skidding velocity); J is the Jacobian of the coordinate transform and is naturally undefined at the distance $n = 1/K$ from the curve, that is, at the local center of curvature of the line. To avoid any singularity, it is imperative that the jet width be much smaller than local curvature radius $1/K$. This is the essence of the thin-jet approximation.

The choice of a narrow jet leads to the following choices for the sizes of the various independent and dependent variables:

alongjet distance and meander displacements:	$s \sim X \sim Y \sim 1/\epsilon$
acrossjet distance:	$n \sim 1$
interfacial depth variations:	$h \sim 1$
alongjet velocity:	$U \sim 1$
acrossjet velocity:	$V \sim \epsilon$
time:	$t \sim 1/\epsilon^2$,

where ϵ is the number, much smaller than unity, that measures the narrowness the jet. The fact that variations in h are on the order of one implies that finite depth variations across the jet (dimensionally as large as H) are allowed. This is in contrast with the quasi-geostrophic studies of Robinson et al. (1975) and Pratt (1988). The velocity and time scales result from educated guesses, such as geostrophy of the along-jet velocity component.

The preceding scales imply $K \sim \epsilon$ or a meander radius of curvature on the order of $1/\epsilon(\gg 1)$. In the subsequent mathematical developments, it will be necessary to integrate certain quantities across the jet, that is, from a large negative to a large positive value of n. In the spirit of boundary-layer theory, a "large" value of n will be meant as much larger than unity (away from the jet) but less than $1/\epsilon$ (not to reach the center of meander curvature).

Although the smallness of ϵ is arbitrary, it must somehow be measured against that of β [see (2.4)–(2.5)]. The richest dynamics are found when $\epsilon^2 \sim \beta$, with planetary dynamics dominating for lesser values of ϵ and meander curvature dominating for larger values. Let us then take $\epsilon = \beta^{1/2}$, which with dimensions implies that the meander length scale L, the radius of deformation R_d, and the planetary parameters are related by

$$L = \left(R_d \frac{f_0}{df/dy} \right)^{1/2}. \tag{2.18}$$

For a deformation radius $R_d = 40$ km and a planetary scale $f_0(df/dy)^{-1} = 3500$ km, the meander length scale is $L \approx 370$ km, a very reasonable meander wavelength and amplitude for the Gulf Stream (Watts and Johns 1982; Tracey and Watts 1986).

Expanding all variables in terms of the small number ϵ, for example,

$$X = X_0 + \epsilon X_1 + O(\epsilon^2),$$

we obtain at leading order the much reduced set of equations:

$$U_0 \frac{\partial U_0}{\partial s} + (V_0 - C_0) \frac{\partial U_0}{\partial n} - V_0 = -\frac{\partial h_0}{\partial s} \tag{2.19}$$

$$+ U_0 = -\frac{\partial h_0}{\partial n} \tag{2.20}$$

$$\frac{\partial}{\partial s}(h_0 U_0) + \frac{\partial}{\partial n}(h_0 V_0) - C_0 \frac{\partial h_0}{\partial n} = 0. \tag{2.21}$$

The middle equation confirms geostrophy in the cross-jet direction, while the first equation shows that the balance in the perpendicular direction is ageostrophic. Elimination of U_0 via (2.20) and an integration of (2.21) with respect to n yields

$$h_0 \left(V_0 - C_0 - \frac{\partial h_0}{\partial s} \right) = p(s, t), \tag{2.22}$$

where the function $p(s, t)$, should be determined by boundary conditions.

Four cases should be distinguished depending on the asymptotic values of h_0, the basic crossjet interfacial profile. These cases are illustrated in Fig. 2. In cases I and II, the interface reaches the surface at least once; there h_0 vanishes, and (2.22) implies $p(s, t) = 0$. A subsequent division by h_0 yields

$$V_0 = C_0 + \frac{\partial h_0}{\partial s}.$$

This is all that can be stated about case I at this stage. For case II, the interface extends to infinity, where, away from meanders, h_0 reaches the asymptotic values h_1, a pure constant. At such large distances from the jet, there can be neither crossjet velocity or variations in the s direction ($V_0 = \partial h_0/\partial s = 0$). The last expression requires that C_0 vanish, and reduces to

$$V_0 = \frac{\partial h_0}{\partial s}. \tag{2.23}$$

In case III, h_0 reaches different asymptotic values, h_1 and h_2, on each side. Expression (2.22) applied at those extremes ($V_0 = \partial h_0/\partial s = 0$) yields

$$-h_1 C_0 = p, \quad -h_2 C_0 = p,$$

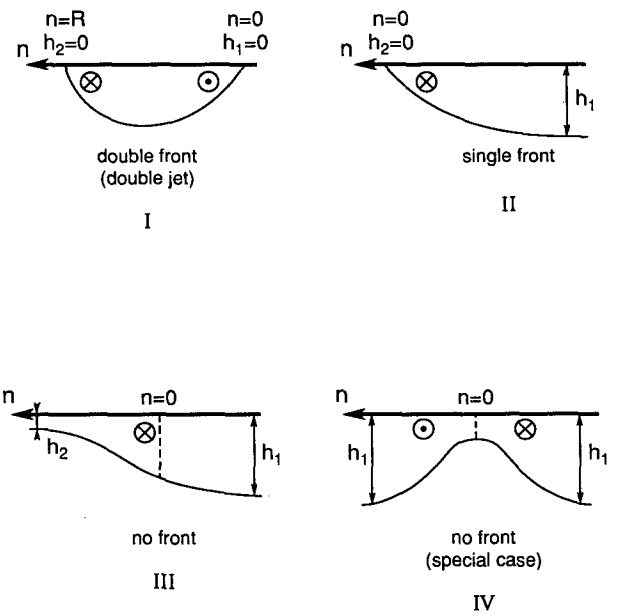

FIG. 2. The four possible profiles of the interfacial displacement across the jet: double front (I), single front (II), and no front (III and IV). In case IV, the asymptotic value of the upper-layer depth is the same on both sides. Cases I and IV correspond to velocity profiles with no mean flow, and do not fall under the present theory. (Current directions are indicated for the Northern Hemisphere only.)

which lead to $p = C_0 = 0$. Again the result is (2.23). In case IV, the asymptotic values are identical; the function p is equal to $-h_1 C_0$, and V_0 is given by

$$V_0 = \frac{\partial h_0}{\partial s} + \left(1 - \frac{h_1}{h_0}\right) C_0.$$

Because the h_0 profiles of cases I and IV correspond to jets with accompanying return flows and no net geostrophic transport, much unlike the Gulf Stream, we wish not to consider these cases further. This leaves us with cases II and III, of which the dynamics at this level are somewhat degenerate. First, C_0 vanishes, and there is no prognostic term left in any of the equations. Moreover, with $V_0 = \partial h_0/\partial s$, Eq. (2.19) becomes

$$\frac{\partial h_0}{\partial s}\frac{\partial^2 h_0}{\partial n^2} - \frac{\partial h_0}{\partial n}\frac{\partial^2 h_0}{\partial s \partial n} = 0.$$

The most general solution to this last equation is

$$h_0 = F[n + q(s, t), t].$$

The arbitrary function $q(s, t)$ can be set to zero since the origin of n has not yet been specified. Physically, this choice amounts to defining the position of the so-called midjet line within the h_0 profile. For example, the origin of the n axis in case II can be conveniently placed at the front, while in case III the inflection point would be a natural choice. The extra, parameteric dependency on time appears unnecessary since the vanishing of C_0 eliminates the presence of the time variable at this stage. As a result, the h_0 profile can only depend on the crossjet coordinate n, and must be interpreted as a frozen profile found at all times and at all positions along the jet. We will consider it as given information regarding the particular jet under consideration. Higher-order dynamics control the small temporal and spatial distortions of the basic profile, as well as the moving and curving of the midjet line onto which the basic profile is attached.

With $\partial h_0/\partial s = 0$, V_0 is nil: the crossjet velocity is then smaller than anticipated. Similarly, the vanishing of C_0 implies a longer time scale than expected. (Note that the last two assertions do not hold in cases I and IV.) The next-order dynamics yield

$$U_0 \frac{\partial U_1}{\partial s} + (V_1 - C_1)\frac{\partial U_0}{\partial n} - V_1 = -\frac{\partial h_1}{\partial s}, \quad (2.24)$$

$$U_1 + Y_0 U_0 + K_0 U_0^2 = -\frac{\partial h_1}{\partial n}, \quad (2.25)$$

$$U_0 \frac{\partial h_1}{\partial s} + (V_1 - C_1)\frac{\partial h_0}{\partial n} + h_0\left(\frac{\partial U_1}{\partial s} + \frac{\partial V_1}{\partial n}\right) = 0. \quad (2.26)$$

Equation (2.25) brings into the formalism the beta and curvature effects (Y_0 and K_0 terms, respectively). We thus anticipate that meandering will be affected by these processes rather than result from intrinsic instabilities of the basic jet profile (which appears to be the fate of jets in cases I and IV).

Elimination of the alongjet velocity perturbation U_1 by use of (2.25) and the recall of the leading-order geostrophic balance (2.20) transform (2.24) and (2.26) into

$$\left(1 + \frac{d^2 h_0}{dn^2}\right)\left(V_1 - \frac{\partial h_1}{\partial s}\right) = \frac{dh_0}{dn}\frac{\partial^2 h_1}{\partial s \partial n} - \frac{d^2 h_0}{dn^2}\frac{\partial h_1}{\partial s} + C_1 \frac{d^2 h_0}{dn^2} - \left(\frac{dh_0}{dn}\right)^2 \frac{\partial Y_0}{\partial s} + \left(\frac{dh_0}{dn}\right)^3 \frac{\partial K_0}{\partial s} \quad (2.27)$$

$$\frac{\partial}{\partial n}\left[h_0\left(V_1 - \frac{\partial h_1}{\partial s}\right)\right] = C_1 \frac{dh_0}{dn} - h_0 \frac{dh_0}{dn}\frac{\partial Y_0}{\partial s} + h_0\left(\frac{dh_0}{dn}\right)^2 \frac{\partial K_0}{\partial s}. \quad (2.28)$$

These two equations form a 2×2 system for h_1 and V_1. A solution, however, will exist only if the second equation meets a certain compatibility equation. Indeed, integrating this second equation (2.28) across the entire range of values of h_0, for example, from large positive n to either $n = 0$ (case II) or large negative n (case III), the left-hand side yields no contribution because either $h_0 = 0$ at the front or V_1 and $\partial h_1/\partial s$ vanish at large distances. It remains

$$C_1 \int \frac{dh_0}{dn}\, dn = \frac{\partial Y_0}{\partial s}\int h_0 \frac{dh_0}{dn}\, dn - \frac{\partial K_0}{\partial s}\int h_0 \left(\frac{dh_0}{dn}\right)^2 dn.$$

Because the integrands in this equation do not exhibit singularities at infinity, the integrals can be extended from $n = -\infty$ to either $n = 0$ or $n = +\infty$. These integrals depend solely on the given crossjet structure, h_0, and can be calculated once and for all. The first two are negative, while the third is positive. A division by the first integral permits one to write

$$C_1 = a\frac{\partial K_0}{\partial s} + b\frac{\partial Y_0}{\partial s}, \quad (2.29)$$

where

$$a = -\frac{\int h_0 \left(\frac{dh_0}{dn}\right)^2 dn}{\int \frac{dh_0}{dn}\, dn}, \qquad b = \frac{\int h_0 \frac{dh_0}{dn}\, dn}{\int \frac{dh_0}{dn}\, dn} \quad (2.30)$$

are two positive coefficients that can be considered as known quantities.

Equation (2.29) is the evolution equation that we were seeking; it relates the velocity of the midjet line

(or front for case II) to a curvature effect and a planetary (beta) effect. Tracing back the curvature term to the momentum equation (2.25), we note that the source of this curvature effect is the centrifugal force acting on the particles as they negotiate meanders.

Collecting Eqs. (2.8), (2.9), and (2.29) and dropping the subscripts that are no longer necessary, we obtain a self-contained set of equations:

$$\left(\frac{\partial X}{\partial s}\right)^2 + \left(\frac{\partial Y}{\partial s}\right)^2 = 1 \tag{2.31}$$

$$K = \frac{\partial X}{\partial s}\frac{\partial^2 Y}{\partial s^2} - \frac{\partial^2 X}{\partial s^2}\frac{\partial Y}{\partial s} \tag{2.32}$$

$$\frac{\partial X}{\partial s}\frac{\partial Y}{\partial t} - \frac{\partial X}{\partial t}\frac{\partial Y}{\partial s} = a\frac{\partial K}{\partial s} + b\frac{\partial Y}{\partial s}. \tag{2.33}$$

A return to dimensional variables leaves these equations unchanged as long as the constants a and b are modified according to

$$a = \frac{g'^2}{f_0^3}\frac{\int h(dh/dn)^2 dn}{h_1 - h_2}, \quad b = \frac{g'(h_1 + h_2)}{2f_0^2}\frac{df}{dy}, \tag{2.34}$$

where h_1 and h_2 are the two limiting values of h (see Fig. 2).

A simple geometrical interpretation of (2.33) can be obtained by considering the motion of an infinitesimal segment of arc moving with velocity $(\partial X/\partial t, \partial Y/\partial t)$. When written in terms of the azimuth θ, measured counterclockwise from the zonal direction, the left-hand side of (2.33),

$$\cos\theta\frac{\partial Y}{\partial t} - \sin\theta\frac{\partial X}{\partial t},$$

is clearly the velocity of the segment normal to itself, with positive values to the left of increasing s. Equation (2.33) therefore indicates that this normal velocity is proportional to the rate of change of centrifugal force along the path $(\partial K/\partial s)$ and the azimuth angle from the zonal direction $(\partial Y/\partial s)$. The former can alternatively be interpreted as a vortex induction effect (Pratt 1988).

Equations (2.31)–(2.33) form a system for the three unknowns, X, Y, and K, that describe the midjet path. Equivalent formulations can be proposed, but we feel that the foregoing one is the most symmetric in its presentation, for it does not discriminate before the X and Y coordinates of the jet axis, except insofar as the beta effect is concerned [b term in (2.33)]. When the beta effect is neglected [$b = 0$ in (2.33)] and when the coordinate s is eliminated leaving X as the independent spatial variable [at the cost of a multivalued $Y(X, t)$ function], we recover exactly the path equation of Pratt (1988).

3. Connection with theory of Flierl and Robinson (1984)

It is natural to ask whether (2.33) is a special case of the path equation derived by FR for a thin, Boussinesq, β-plane jet over a horizontal bottom. Surprisingly, the answer is no: Eq. (2.33) contains a term not included in the (apparently) more general result of FR. It *is* possible, however, to recover (2.33) by making slight alterations in the derivation of FR. The general procedure is sketched below.

One of the key simplifications in the FR theory is the assumption that the jet path is independent of z. Under this condition the velocity normal to the jet axis must be independent of z, and therefore, baroclinic motions are severely limited. The most obvious implication is that baroclinic instability, whereby the cross-stream slope of isopycnals is decreased, is eliminated. In the present 1 1/2-layer model baroclinic motions are retained (although baroclinic instability is absent). The jet path extends only through the upper layer, and the weak normal velocity in the lower layer is opposite in sign to its upper-layer counterpart.

In more specific terms, the derivation of FR is based on integration of the vorticity equation [their Eq. (4)], which contains a stretching term ($\partial w/\partial z$ in their notation). Integration over the water column leads to a null result, since w vanishes at the upper and lower boundaries. With 1 1/2-layer stratification, however, the integration takes place over the vertical extent of the active layer, and a finite contribution arises due to the nonzero vertical velocity at the density interface. This contribution eventually leads to the left-hand side of Eq. (2.33), the missing terms alluded to earlier.

If the derivation is carried forth using the previously outlined step, a slightly more complicated version of the result obtained by FR will result. Recovery of (2.33) can then be made by taking a limit in which the ratio of meander phase speed to parcel speed in the jet is forced to be much smaller than the other dimensionless parameters. This last step is appropriate for 1 1/2-layer models and is tantamount to elimination of the barotropic mode.

The preceding discussion does not imply that an error was made by FR. Repetition of their analysis (including integration over the entire water column) using 1 1/2-layer stratification simply results in an indeterminate system. Additional information would be required to calculate the vertical structure of the flow.

4. Special solutions and limiting cases

a. Straight lines

Before considering the general time-dependent behavior of (2.33) we first investigate some special cases. First, consider a solution consisting of a straight line

($K = 0$) inclined at an angle θ_0 with respect to the x axis. Equation (2.33) then reduces to

$$\cos\theta_0 \frac{\partial Y}{\partial t} - \sin\theta_0 \frac{\partial X}{\partial t} = b \sin\theta_0;$$

that is, the velocity of the front normal to itself is equal to $b \sin\theta_0$. When the path is aligned east–west ($\theta_0 = 0$) the path is stationary. For north–south alignment the path translates westward at speed b. The same phenomenon is observed in the calculation of Pedlosky (1990).

b. *Steady states*

Next, consider a purely stationary ($\partial X/\partial t = \partial Y/\partial t = 0$) solution for which (2.33) reduces to

$$K = -\frac{b}{a} Y + \text{const.} \qquad (4.1)$$

This equation, derived by Robinson and Niiler (1967), was subsequently used by Masuda (1982) to study the bimodal character of the Kuroshio. Solutions to (4.1) consist of stationary meander patterns in which eastward advection by the jet is balanced by westward propagation tendencies induced by local vortex induction and the β effect. When $b = 0$ the solutions reduce to circles ($K = \text{const}$).

c. *Periodic meanders of permanent form*

The only straight-line solution that is also a steady state is that of east–west alignment. We now look for plane-wave solutions consisting of perturbations of this basic state. Let the natural coordinate system be imbedded such that any point (X, Y) on the front remains fixed in a frame of reference moving with steady eastward phase speed c. Then $\partial X/\partial t = c$, $\partial Y/\partial t = 0$, $\partial X/\partial s = \cos\theta$, $\partial Y/\partial s = \sin\theta$, and (2.33) reduces to

$$\frac{\partial^2\theta}{\partial s^2} + \frac{(c+b)}{a} \sin\theta = 0. \qquad (4.2)$$

This is simply the nonlinear pendulum equation; the solutions of which have been obtained and transformed to Cartesian coordinates by Pratt (1988). In his f-plane, quasigeostrophic analysis, the coefficient of the $\sin\theta$ term is $2c$ and generalization to the present case can be made by replacing $2c$ by $(c + b)/a$. The results are shown in Fig. 3 (essentially a copy of his Fig. 3 with the appropriate label replacements). Curves of constant $(c + b)/a$ are shown in meander wavenumber and amplitude space. For specified values of a and b, Fig. 3 constitutes a nonlinear dispersion relation for the meanders in which c is given by the Cartesian wavenumber k and amplitude A. The meanders are multivalued for $kA > 2.61$ (lower dashed line) and self-intersecting for $kA > 8.30$ (upper dashed line).

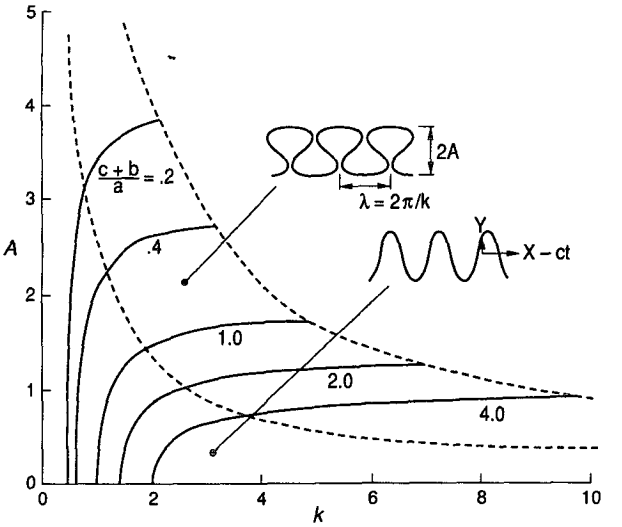

FIG. 3. Nonlinear dispersion relation for periodic, finite-amplitude meanders. The solid curves indicate constant values of $(c + b)/a$ and are plotted as a function of the meander wavenumber k and amplitude A. The dashed lines separate regions of single-valuedness, multivaluedness, and self-intersection. The lower and upper dashed lines are given by $kA = 2.61$ and $kA = 8.30$, respectively.

If the parameter $(c + b)/a$ in Eq. (4.2) is eliminated by rescaling the coordinate s by factor $(c + b)^{1/2}/a^{1/2}$, the solutions collapse to a single curve. The latter is simply the $(c + b)/a = 1$ curve in Fig. 3, with appropriately rescaled wavenumber and amplitude. To avoid confusion, this result is reproduced in Fig. 4. The single curve shows the value of $(b + c)^{1/2}A/a^{1/2}$ determined by given $a^{1/2}k/(b + c)^{1/2}$, or vice versa. Although this plot elegantly shows the self-similarity contained in the solutions, it does not easily allow determination of phase speed for given wavelength and amplitude. Figure 3 should be used for the latter.

In addition, setting $c = 0$ gives the threshold value of amplitude separating downstream ($c < 0$) from retrograde ($c < 0$) propagation at a given k. As k increases, so does the threshold amplitude. When $c = 0$, solutions lying along the curve correspond to stationary meanders, identical to the steady states discussed by Masuda (1982).

Finally, if we restrict attention to small amplitude oscillations ($\theta \ll 1$), so that $\sin\theta \to \theta$ in (4.2), the solution $\theta = A \sin kx$ leads to the linear dispersion relation

$$c = ak^2 - b. \qquad (4.3)$$

Stationary meanders thus occur at wavenumber $k = (b/a)^{1/2}$, as indicated in Fig. 4. Longer waves propagate westward (upstream), while shorter waves travel downstream. Note that the group velocity

$$c_g = 3ak^2 - b$$

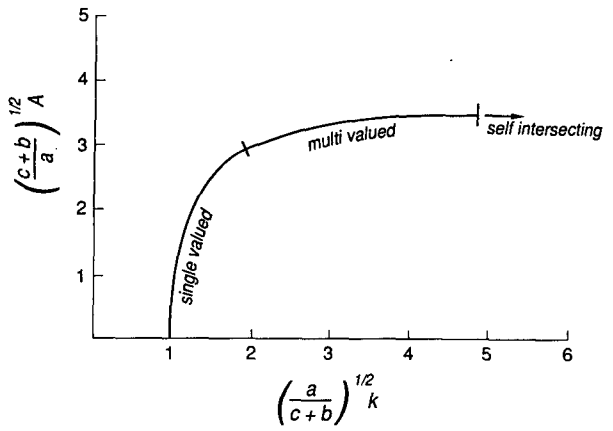

FIG. 4. The dispersion of information from Fig. 3 has been collapsed into the single curve shown here.

has value $2b$ for the stationary meanders, indicating eastward energy flux.

5. Solitons, breathers, and the mKdV equation

We now turn to initial-value and initial–boundary value problems. In this context the form of (2.33) is rather inconvenient, and we seek to obtain an equivalent representation containing the single dependent variable θ, the local azimuth of the jet.

Using the relationships $\partial X/\partial s = \cos\theta$, $\partial Y/\partial s = \sin\theta$, $K = \partial\theta/\partial s$, (2.33) can be rewritten

$$\sin\theta \frac{\partial X}{\partial t} - \cos\theta \frac{\partial Y}{\partial t} = -a \frac{\partial^2 \theta}{\partial s^2} - b \sin\theta. \quad (5.1)$$

Successive differentiations with respect to s yield

$$\cos\theta \frac{\partial X}{\partial t} + \sin\theta \frac{\partial Y}{\partial t} = \frac{\dfrac{\partial\theta}{\partial t} - a \dfrac{\partial^3\theta}{\partial s^3} - b \dfrac{\partial\theta}{\partial s}\cos\theta}{\dfrac{\partial\theta}{\partial s}}, \quad (5.2)$$

and

$$-\sin\theta \frac{\partial X}{\partial t} + \cos\theta \frac{\partial Y}{\partial t} = \frac{\partial\theta}{\partial s}\frac{\partial}{\partial s}\frac{\left(\dfrac{\partial\theta}{\partial t} - a \dfrac{\partial^3\theta}{\partial s^3} - b \dfrac{\partial\theta}{\partial s}\cos\theta\right)}{\dfrac{\partial\theta}{\partial s}}. \quad (5.3)$$

Adding (5.1) and (5.3), multiplying the result by $\partial\theta/\partial s$, and integrating once with respect to s leads to

$$\frac{\partial\theta}{\partial t} = a \frac{\partial^3\theta}{\partial s^3} + \frac{1}{2} a\left(\frac{\partial\theta}{\partial s}\right)^3 + c_0(t) \frac{\partial\theta}{\partial s}. \quad (5.4)$$

The function $c_0(t)$ is determined by boundary or initial conditions. For example, consider the case in which the path is held fixed at one end ($s = 0$, say) and the angle $\theta(0, t)$ and curvature $\partial\theta(0, t)/\partial s$ are prescribed. Evaluating (5.2) and (5.4) at $s = 0$, where $\partial X/\partial t = \partial Y/\partial t = 0$, and combining the results leads to

$$c_0 = b \cos\theta(0, t) - \frac{1}{2} a\left[\frac{\partial\theta}{\partial s}(0, t)\right]^2.$$

If, instead, $\theta(s, 0)$ is prescribed over $-\infty < s < \infty$ such that $\theta(s, 0) \to 0$ as $s \to -\infty$, the above arguments lead to $c_0 = b$.

If, in this latter case, (5.4) is differentiated with respect to s and the scaled variables

$$\tau = a^{-1/2} t$$

$$\kappa = \frac{1}{2} a^{1/2} \frac{\partial\theta}{\partial s}$$

$$\xi = -a^{-1/2}[s + bt]$$

are introduced, the modified Korteweg–deVries (mKdV) equation,

$$\frac{\partial\kappa}{\partial\tau} + 6\kappa^2 \frac{\partial\kappa}{\partial\xi} + \frac{\partial^3\kappa}{\partial\xi^3} = 0, \quad (5.5)$$

is obtained. Initial-value problems in Cartesian space can now be solved using standard techniques (Lamb 1980; Ablowitz et al. 1974) by imposing the equivalent initial condition $\kappa(\xi, 0)$ on (5.5).

Equation (5.5) admits the single-soliton solution,

$$\kappa = \pm 2k \operatorname{sech}(2k\xi - 8k^3\tau + \delta)$$

or, in the previous coordinates,

$$\frac{\partial\theta}{\partial s} = \pm 4ka^{-1/2} \operatorname{sech}\{-2ka^{-1/2}(s + bt) - 8k^3 a^{-1/2} t + \delta\}. \quad (5.6)$$

As one moves from $s = -\infty$ to $s = \infty$, the net change in θ experienced by this wave form is $\pm 2\pi$, indicating that a "loop" is executed. In fact, the solution consists of the single loop propagating with speed $ds/dt = -(b + 4k^2)$. A Cartesian representation of the loop soliton is given in Fig. 5a.

It should be noted that a single-loop soliton cannot evolve from a single-valued initial condition without a cusp first occurring in the path (Fig. 5b). Two loop solitons, one inside the other, could form without such singularity (Fig. 5c). Proof of this behavior can be shown by integration of (5.5) over all ξ, leading to

$$\frac{d}{dt}\int_{-\infty}^{\infty} \kappa d\xi = \frac{1}{2} a^{1/2}(\theta(\infty, t) - \theta(-\infty, t)) = 0.$$

If $\theta(\infty, 0) = \theta(-\infty, 0)$, loop solitons can arise only in negative and positive pairs; otherwise, the difference $\theta(\infty, t) - \theta(-\infty, t)$ will be finite.

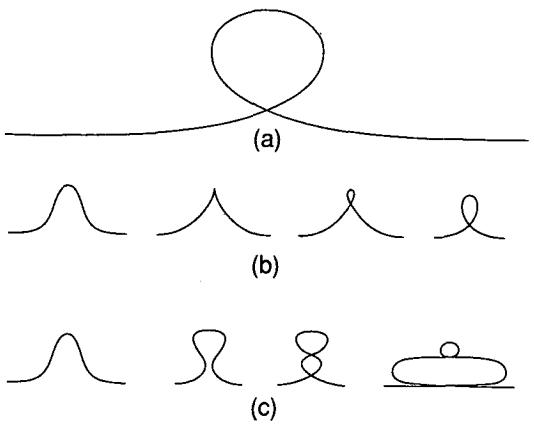

FIG. 5. Schematic depiction of loop soliton (a), the formation of a loop soliton with intermediate cusp formation (b), and the formation of two superimposed loop solitons in a figure-eight configuration (c). In (b) and (c), time increases as one moves to the right through successive frames.

A second and more physical wave form admitted by (5.5) is an envelope solitary wave or "breather" (Lamb 1980):

$$\kappa = -2\frac{\partial}{\partial\xi}\tan^{-1}\left[\frac{\lambda\sin(2\alpha\xi + \delta\tau - \Theta_p)}{\cosh(2\lambda\alpha\xi + \gamma\tau + \Theta_e)}\right],$$

where α and λ are arbitrary parameters and δ and γ are given by

$$\delta = 8\alpha^3(1 - 3\lambda^2)$$
$$\gamma = 8\alpha^3\lambda(3 - \lambda^2).$$

The breather is a packet of waves propagating inside an envelope of permanent form. When expressed in terms of previous variables, the solution is described by

$$\theta = 4\tan^{-1}\left(\frac{\lambda\sin[-2\alpha a^{-1/2}s + a^{-1/2}(2\alpha c_0 + \delta)t - \Theta_p]}{\cosh[-2\alpha\lambda a^{-1/2}s + a^{-1/2}(2\lambda\alpha c_0 + \gamma)t + \Theta_e]}\right)$$

with $c_0 = -b$. The envelope (corresponding to the cosh term) propagates with speed $c_e = c_0 + \gamma/2\alpha\lambda = 4\alpha^2(3 - \lambda^2) - b$, while the interior oscillations (corresponding to the sin term) have speed $c_p = c_0 + \delta/2\alpha = 4\alpha^2(1 - 3\lambda^2) - b$. The constants Θ_p and Θ_c determine the phase lags between the envelopes, oscillations, and origin.

The free parameters α and λ determine the length scales $a^{1/2}/2\alpha\lambda$ and $a^{1/2}/2\alpha$ of the envelope and oscillations. As $\lambda \to 0$, the steepness of the breather and its amplitude decrease and the solution takes the form of small amplitude, uniform wave train. In this limit the phase speed c_p of the oscillations approaches the previously noted linear value $4\alpha^2 - b = ak^2 - b$, with $k = 2\alpha a^{-1/2}$. For $\lambda > \tan(\pi/8)$, the maximum value of θ exceeds $\pi/2$, and thus, the breather becomes multivalued (in a Cartesian sense). If λ exceeds unity, intersections between different path segments occur and the solution becomes invalid. Figure 6 shows the case $\lambda = 1$, for which grazing contact first appears. The different contours show realizations of the same breather at different phases $t = 0, T/8, T/4$, etc., where T is the period of the interior oscillations. As shown, the path experiences self-intersections only at $t = 0, T/2, T$, etc., in contrast to the loop soliton.

As described by Lamb (1980), the initial-value problem for Eq. (5.5) can be solved using the inverse scattering technique. Furthermore, the number of solitons and breathers that evolves from an isolated initial distribution of κ can be determined directly from the scattering coefficient, along with the corresponding values of λ. Should any loop solitons (or breathers with $\lambda \geq 1$) arise, then it is clear that self-intersection of the path must occur at some finite time. Such an event presumably marks the onset of detachment of a segment of the path, as in the formation of a "ring." Of course, the thin-jet approximation is violated at this point, and no further integration of the governing equation is permissible. These considerations suggest that eddy detachment, or lack thereof, might be predicted analytically by computing the scattering coefficients associated with the initial data. This problem

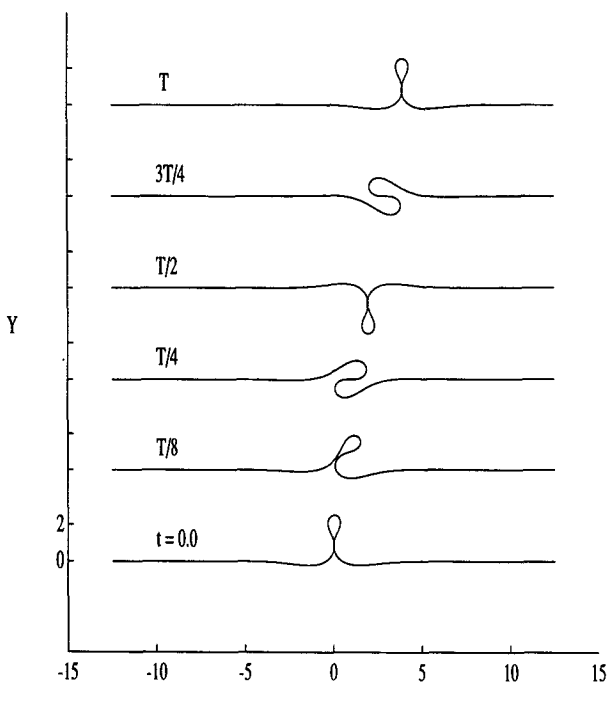

FIG. 6. Evolution of breather with $\alpha = 0.4$ and $\lambda = 1.0$ over one period ($T = 3.07$).

has been considered by Ralph (1991) and will be the subject of a subsequent paper.

6. Numerical examples

To illustrate the emergence of breathers from an initially isolated meandering disturbance, Eq. (5.4) has been solved numerically, using a finite-difference method. Center differencing is applied in space. Time stepping is carried out using a predictor–corrector method, with a leapfrog scheme to predict and a trapezoidal integration to correct. The resultant scheme is second order in space and time, and conditionally stable when

$$\Delta t \leq \sqrt{2}\left[\frac{|a|}{\Delta s^3} + \frac{|b|}{\Delta s}\right]^{-1}.$$

[An alternative approach is to solve (5.5) numerically, which can be done using pseudospectral methods (Fornberg and Whitham 1978)].

Two examples are given: the first of which shows the development of a nonlooped breather. The initial condition is

$$\theta(s, 0) = 3.6\ \mathrm{sech}(2s)\tanh(2s), \qquad (6.1)$$

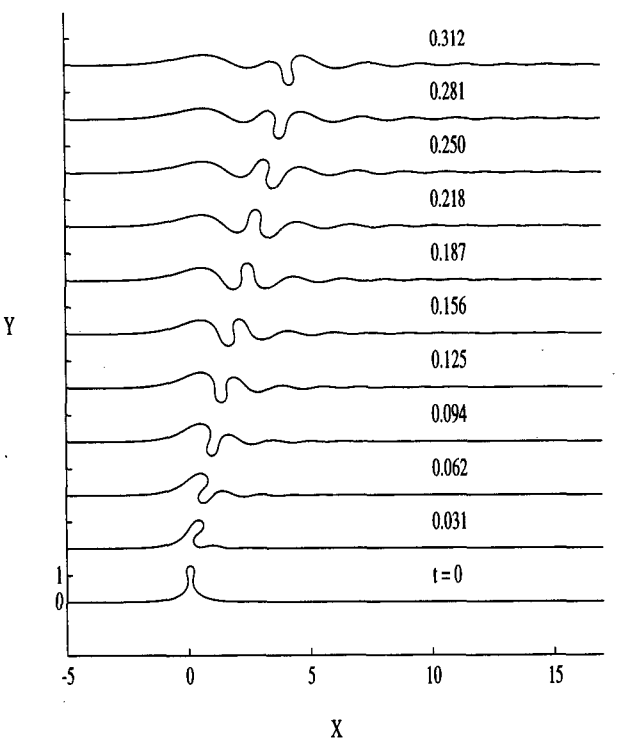

FIG. 7. Numerical evolution for an initial thin lobe given by (6.1).

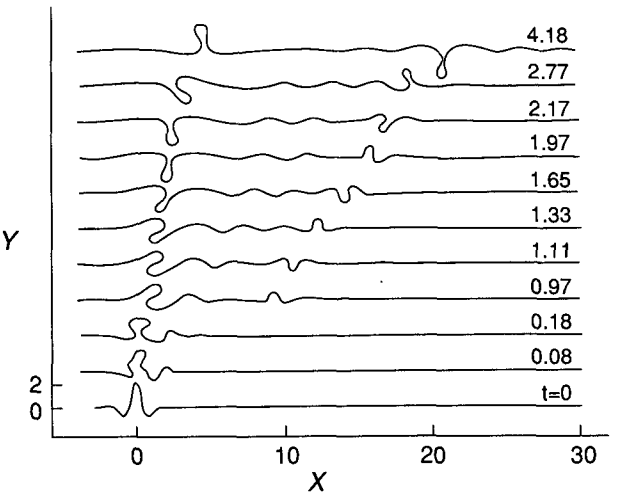

FIG. 8. Formation of two breathers using the initial condition given by (6.2) (from Pratt 1988).

and Fig. 7 shows the evolution leading to an isolated wave packet. The second example, taken from Pratt (1988), is based on the initial condition,

$$Y(X, 0) = 2e^{-X^2}\cos(3X), \qquad (6.2)$$

where Y denotes the y position of the front. Two breathers emerge, the first centered near $X = 3$ and the second near $X = 20$ in the $t = 4.18$ profile shown in Fig. 8. The latter produced a closed loop. The Fig. 8 results were obtained before the connection with the mKdV equation was discovered.

7. Estimation of parameters from Gulf Stream data

Estimates of the model parameters a and b were made using a Gulf Stream density cross section taken at 68°W by Hall and Fofonoff (1992). The parameters were computed by using an isopycnal to represent the shape of the interface in the 1 1/2-layer model stratification. Five estimates were made using the isopycnals indicated in Fig. 9 (from their paper). Two of the isopycnals, $\sigma_\theta = 26.5$ and $\sigma_\theta = 26.6$, outcrop, defining the northern edge of the stream. For nonoutcropping isopycnals, the edges of the stream were chosen to be where the isopycnal slope was judged zero. The depth of the isopycnal was scaled by H, the depth of that isopycnal on the southern edge of the Gulf Stream. Values of H range from 550 m for the 26.5 contour to 1330 m for the 27.7 contour. Cross-stream distances were nondimensionalized using $R_d = \sqrt{(g'H)}/f_0$ with $f_0 = 9.4 \times 10^{-5}\ \mathrm{s}^{-1}$. The reduced gravity was calculated according to

$$g' = g\left(\frac{\rho_0 - \rho_1}{\rho_0}\right),$$

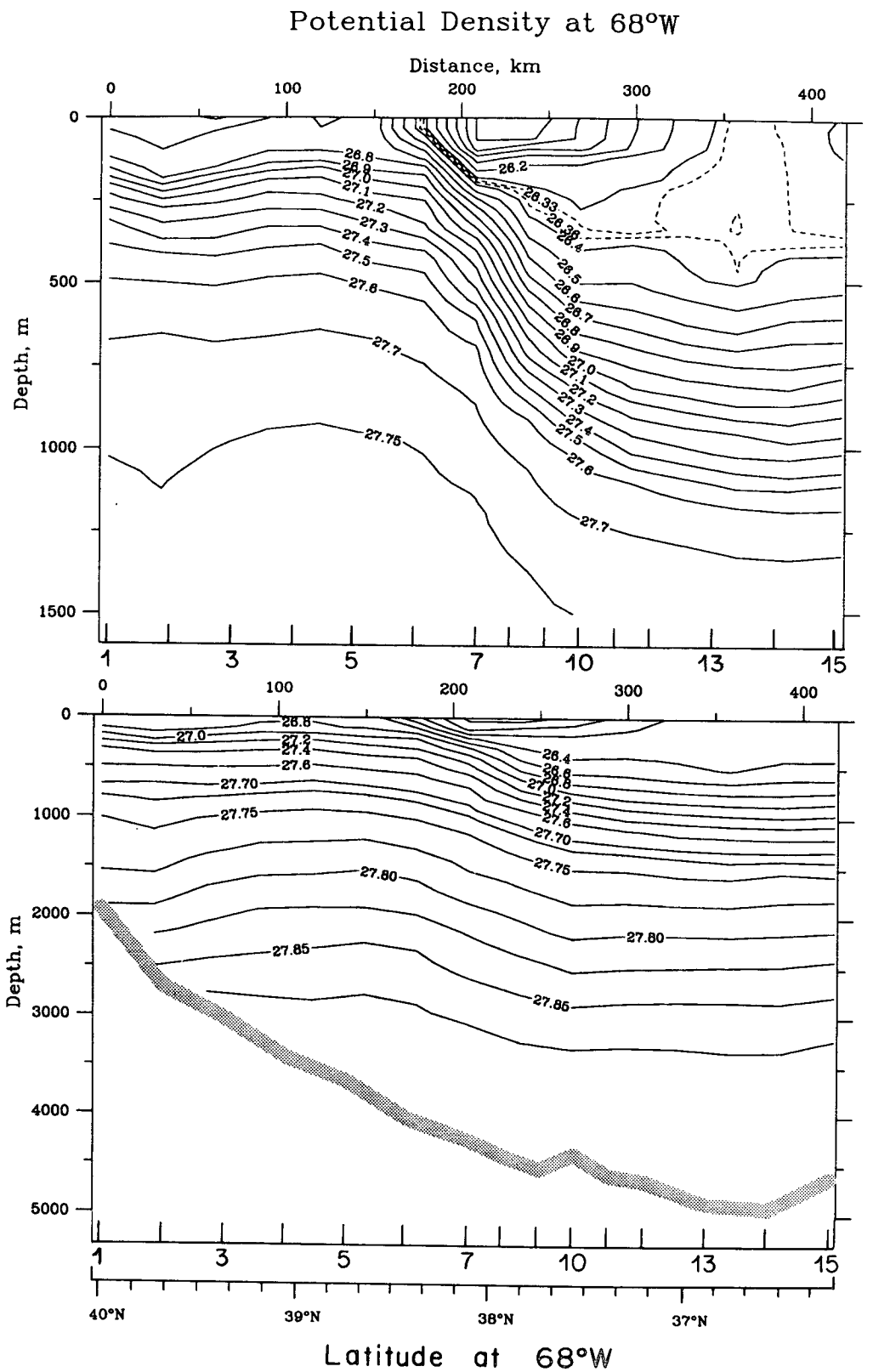

FIG. 9. Density section across the Gulf Stream at 68°W. (From Hall and Fofonoff 1991).

where ρ_0 is the density of the lower layer and ρ_1 is the density of the upper layer. The densities for each layer were estimated by separately averaging the density of the water above and below the isopycnal. The deformation radius for all five of the isopycnals was found to be approximately 40 km.

Once the isopycnal profiles were nondimensionalized, a and b were calculated using integrals (2.30). Table 1 contains the values of a and b for each of the five isopycnals. The parameter b depends on whether the isopycnal outcrops or not. For outcropping isopycnals, $b = 0.5$. As the isopycnals get deeper, b increases to approximately 0.7. The upper two outcropping isopycnals and the two middle isopycnals have $a \approx 0.15$. The 27.7 isopycnal has a much lower value of a ($a = 0.09$). This isopycnal is slightly deeper than the core of the current, so its slope $\partial h/\partial n$ is smaller than the other isopycnals, leading to a smaller estimate of a. Because this isopycnal misses the current core, it is not a good choice for the shape of the interface. These estimates show that interfaces that outcrop do not behave significantly differently than those that do not.

Table 1 suggests that, on average, b exceeds a by a factor of 5. To interpret this result, consider the strength of the restoring tendency associated with the β effect, as measured by

$$\frac{b\cos\theta_0}{ak^2} = \frac{b\cos\theta_0 df/dy}{ak_d^2 f_0 R_d},$$

the ratio of the two terms on the right-hand side of the linear dispersion relation (4.3). Using $b/a = 5, f_0(df/dy)^{-1} = 3500$ km, $R_d = 40$ km, $\cos\theta_0 = 1$, the preceding ratio is unity for wavelength $(2\pi/k_d) \approx 1050$ km. Just off Cape Hatteras where the azimuth of the Gulf Stream is about 30° ($\cos\theta_0 = 0.866$), the critical wavelength is 1130 km. This is the meander scale over which the westward propagation tendency associated with β balances the eastward propagation produced by the combination of advection and local vortex induction. Longer wavelengths propagate westward, while shorter wavelengths move eastward. Lee and Cornillon (personal communication) have identified westward-propagating Gulf Stream meanders having wavelengths in the range from 450 to 2000 km.

TABLE 1. Estimates of a and b.

σ_θ	R_d	a	b
26.5	40.7	0.149	0.50
26.6	42.0	0.150	0.50
27.4	42.6	0.144	0.64
27.6	39.8	0.150	0.70
27.7	36.8	0.099	0.75

8. Conclusions

From the one-layer, reduced-gravity model and the thin-jet approximation, we have extended the Pratt and Stern (1986) path equation to include nonquasigeostrophic dynamics, the beta effect, and continuous potential-vorticity distributions. The equations differ from the fundamentally barotropic path equations derived earlier by Robinson and Niiler (1967) and Flierl and Robinson (1984).

Clearly, our new path equation retains two mechanisms governing the temporal evolution of meanders, and for an eastward jet such as the Gulf Stream, these mechanisms oppose each other. On one hand, the combination of advection and vortex induction (described by Pratt 1988) generates a tendency toward downstream propagation of disturbances, while on the other hand, the beta effect and the attending Rossby-wave dynamics induce a westward propagation, that is, upstream. At a threshold wavelength, meanders are stationary. The existence of such nonpropagating meanders may explain the node observed in the Gulf Stream path some 600 km downstream of Cape Hatteras (Halliwell and Mooers 1983; Cornillon 1986). Indeed, the position of this node may correspond to a distance equal to half the threshold wavelength from the geographically imposed node at Cape Hatteras.

The path equation also admits a variety of steadily translating wave forms, including a periodic wave, a loop soliton, and an envelope soliton or "breather." The latter were found by recasting the path equation as the modified KdV equation. Numerical evidence suggests that meander detachments are associated with the solitons (see Fig. 8). Since the number and connectiveness (intersecting or nonintersecting) of solitons emerging from an arbitrary, isolated initial disturbance can be obtained through a straightforward calculation, the detachment of meanders might be forecast without actually integrating the time-dependent equations. The results of such calculations will be reported in the future.

A final note on the limits of the model is in order. Because of its thin-jet formulation, the present model is unable to represent correctly the eddy pinch-off process. More importantly, our path equation, like all its predecessors, excludes baroclinic instability, which is known to contribute greatly to meander generation and growth. Thus, the preceding equation is not to be interpreted as a low-order forecasting tool, but only as the basis for the elucidation of curvature and beta dynamics in well-defined jets, such as the Gulf Stream.

Acknowledgments. This work was supported by the Office of Naval Research under Grants N00014-91-J-1781 to Dartmouth College and N00014-89-J-1182 to the Woods Hole Oceanographic Institution and by the National Science Foundation under Grant OCE-9115359 to the Woods Hole Oceanographic Institution. The authors wish to thank Dr. Benyang Tang for help-

ful discussions in the early stages of this research and Anne-Marie Michael for typing the manuscript.

REFERENCES

Ablowitz, M. J., D. J. Kaup, A. C. Newell, and H. Segur, 1974. The inverse scattering transform—Fourier analysis for nonlinear problems. *Stud. Appl. Math.*, **53,** 249–315.

Cornillon, P., 1986: The effect of New England seamounts on Gulf Stream meandering as observed from satellite IR imagery. *J. Phys. Oceanogr.*, **16,** 386–389.

Flierl, G. R., and A. R. Robinson, 1984. On the time-dependent meandering of a thin jet. *J. Phys. Oceanogr.*, **14,** 412–423.

Fornberg, B., and G. B. Whitham, 1978. A numerical and theoretical study of certain nonlinear wave phenomena. *Proc. Roy. Soc. London,* **289,** 373–404.

Hall, M. M., and N. P. Fofonoff, 1992. Downstream development of the Gulf Stream from 63° to 55°W. *J. Phys. Oceanogr.*, submitted.

Halliwell, G. R., and C. N. K. Mooers, 1983: Meanders of the Gulf Stream downstream from Cape Hatteras 1975–1978. *J. Phys. Oceanogr.*, **13,** 1275–1292.

Haltiner, G. J., and R. T. Williams, 1980: *Numerical Weather Prediction and Dynamic Meteorology.* Wiley, 477 pp.

Lamb, G. L., 1980. *Elements of Soliton Theory.* Wiley, 289 pp.

Masuda, A., 1982. An interpretation of the biomodal character of the stable Kuroshio path. *Deep-Sea Res.*, **29A,** 471–484.

Pedlosky, J., 1990. On the propagation of velocity discontinuities on potential vorticity fronts. *J. Phys. Oceanogr.*, **20,** 235–240.

Pratt, L. J., 1988. Meandering and eddy detachment according to a simple (looking) path equation. *J. Phys. Oceanogr.*, **18,** 1627–1640.

——, and M. E. Stern, 1986. Dynamics of potential vorticity fronts and eddy detachment. *J. Phys. Oceanogr.*, **16,** 1101–1120.

Ralph, E., 1991. Predicting eddy detachment from thin jets. WHOI/MIT Joint Program Masters Thesis, 105 pp.

Robinson, A. R., and P. P. Niiler, 1967. The theory of free inertial jets: I. Path and structure. *Tellus,* **19,** 269–291.

——, J. R. Luyten, and G. Flierl, 1975. On the theory of thin rotating jets: A quasi-geostrophic time-dependent model. *Geophys. Fluid Dyn.*, **6,** 211–244.

Tracey, K. L., and D. R. Watts, 1986. On Gulf Stream meander characteristics near Cape Hatteras. *J. Geophys. Res.*, **91,** 7587–7602.

Warren, B. A., 1963. Topographic influences on the path of the Gulf Stream. *Tellus,* **15,** 167–183.

Watts, D. R., and W. E. Johns, 1982. Gulf Stream meanders: Observations on propagation and growth. *J. Geophys. Res.*, **87,** 9467–9476.